

01 Aug 2019

Inverse Design of Long-Range Intensity Correlation in Scattering Media

M. Koirala

R. Sarma

H. Cao

Alexey Yamilov

Missouri University of Science and Technology, yamilov@mst.edu

Follow this and additional works at: https://scholarsmine.mst.edu/phys_facwork



Part of the [Physics Commons](#)

Recommended Citation

M. Koirala et al., "Inverse Design of Long-Range Intensity Correlation in Scattering Media," *Physical Review B*, vol. 100, no. 6, American Physical Society (APS), Aug 2019.

The definitive version is available at <https://doi.org/10.1103/PhysRevB.100.064203>

This Article - Journal is brought to you for free and open access by Scholars' Mine. It has been accepted for inclusion in Physics Faculty Research & Creative Works by an authorized administrator of Scholars' Mine. This work is protected by U. S. Copyright Law. Unauthorized use including reproduction for redistribution requires the permission of the copyright holder. For more information, please contact scholarsmine@mst.edu.

Inverse design of long-range intensity correlation in scattering media

M. Koirala,¹ R. Sarma,² H. Cao,² and A. Yamilov^{1,*}

¹*Department of Physics, Missouri University of Science and Technology, Rolla, Missouri 65409, USA*

²*Department of Applied Physics, Yale University, New Haven, Connecticut 06520, USA*



(Received 9 May 2019; revised manuscript received 26 July 2019; published 12 August 2019)

We demonstrate a possibility of using geometry to deterministically control nonlocal correlation of waves undergoing mesoscopic transport through a disordered waveguide. In case of nondissipative medium, we find an explicit relationship between correlation and the shape of the system. Inverting this relationship, we realize inverse design: we obtain specific waveguide shape that leads to a predetermined nonlocal correlation. The proposed technique offers an approach to coherent control of wave propagation in random media that is complementary to wave-front shaping.

DOI: [10.1103/PhysRevB.100.064203](https://doi.org/10.1103/PhysRevB.100.064203)

I. INTRODUCTION

Diffusion is a common description of the typical wave propagation [1–4] in a scattering medium that disregards the phase and, thus, the effects of interference. Persistent interference phenomena lead to universal conductance fluctuations, weak localization corrections, enhanced backscattering, and nonlocal mesoscopic correlations [5–8] that can be captured using the diagrammatic perturbation technique [3,9–11]. The perturbation building block, which describes an interference of two scattering paths, is known as “quantum crossing,” or Hikami box [12,13]. The crossing, see Fig. 1, is a local object confined to a volume ℓ^d , where ℓ is the transport mean free path and d is the dimensionality of the system. This locality of the interference event means that it is independent of the exact shape of the considered geometry. In contrast, propagation between the source of waves to the interference site and on to the detector does depend on the geometry of the system, as seen from Fig. 1. It is described in terms of the ladder propagator, which is in essence a Green’s function $G(\mathbf{r}, \mathbf{R})$ of the diffusion equation for the disorder-averaged intensity. Consequently, to describe the wave interference effects, the knowledge of $G(\mathbf{r}, \mathbf{R})$ in the particular geometry is crucial.

In this work, we derive expressions for the Green’s function in the two- and three-dimensional disordered waveguides with an arbitrary shape in order to obtain the nonlocal long-range mesoscopic correlations [9,14–21]. We adapt the projection technique, developed in physical chemistry for the particle diffusion in confined geometries [22,23], to describe wave diffusion. We reduce the problem to one dimension and obtain analytical solution. We further extend the projection technique to include the effects of absorption commonly encountered in experiments with the electromagnetic waves.

Spatial light modulator and related technologies have enabled manipulation of light propagation in scattering media via shaping the incident wave-front field to tailor it to the specific configuration of scatters in the sample [8,24,25]. This

brought renewed attention to the nonlocal correlations as they were found to be related to such transport parameters as focusing contrast inside the medium [26] and energy deposition [20,23,27–35]. The long-range correlation also affects total transmission via an optimized wave front with a limited degree of input control [21]; it is also a key factor determining the broadband transmission achievable in wave-front shaping [36]. Our derived analytical relation between the long-range correlation and the shape of the waveguide enables the inverse design: selecting the specific waveguide to obtain the desired correlation profile. Therefore, our work opens up additional avenues for coherent control of wave propagation in diffusive scattering media. In recent works [20,35,37,38], we fabricated two-dimensional disordered photonic waveguides with various geometries, which can be used to experimentally test the presented results.

II. PROJECTION TECHNIQUE

In this section we outline the projection technique that allows one to reduce the two- or three-dimensional diffusion problem to one dimension. For completeness, in this section we will consider time-dependent diffusion and will also include the effect of absorption.

We define the Green’s function $G(\mathbf{r}, \mathbf{r}')$ of the diffusion equation via the equation

$$\frac{\partial G(\mathbf{r}, \mathbf{r}', t)}{\partial t} - D_0 \nabla_{\mathbf{r}}^2 G(\mathbf{r}, \mathbf{r}', t) + \frac{G(\mathbf{r}, \mathbf{r}', t)}{\tau_a} = S_0(t) \delta(\mathbf{r} - \mathbf{r}'), \quad (1)$$

where D_0 is the diffusion constant and τ_a is the absorption time. Note that unlike the more conventional definition, we retain a generic expression for intensity $S_0(t)$ at the point source at \mathbf{r}' . In context of light scattering, $G(\mathbf{r}, \mathbf{r}')$ represents an ensemble-averaged intensity at \mathbf{r} in the medium with the source at \mathbf{r}' . The geometry of the three-dimensional (3D) system is schematically depicted in Fig. 1, with $0 \leq z \leq L$, $x^2 + y^2 \leq [W(z)/2]^2$ in three dimensions or $-W(z)/2 \leq y \leq W(z)/2$ in two dimensions, where $W(z)$ is the diameter of the waveguide. The corresponding cross section area $A(z)$ is

*yamilov@mst.edu

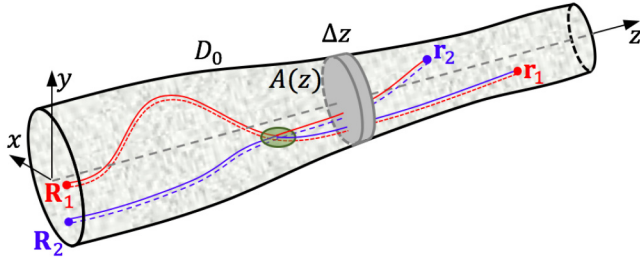


FIG. 1. Schematic depiction of a disordered waveguide with varying diameter. In diagrammatic description of wave transport, the long-range correlation between intensities at \mathbf{r}_1 and \mathbf{r}_2 arises when two propagation paths, described by the Green's function of diffusion equation, intersect allowing a swap of field amplitudes.

$\pi W^2(z)/4$ in three dimensions and $W(z)$ in two dimensions. The boundary conditions consist of the reflection (zero flux) condition $\partial G(\mathbf{r}, \mathbf{r}', t)/\partial \mathbf{n} = 0$ at the walls of the waveguide and open boundary conditions at the two ends ($z = 0, L$), $[z_0 \partial G(\mathbf{r}, \mathbf{r}', t)/\partial z \mp G(\mathbf{r}, \mathbf{r}', t)]_{z=0,L} = 0$, where $z_0 = (\pi/4)\ell$ is the extrapolation length [1]. We note that the above description of wave propagation implicitly assumes that the diffusion description is applicable. This assumption involves the following conditions [3,11]: (i) $k \times \ell \gg 1$, where k is the wave number and ℓ is the transport mean free path; (ii) $W(z), L \gg \ell$; and (iii) $g \gg 1$, where g is the dimensionless conductance of the system, which will be related to $k, \ell, W(z)$ and L below. Condition (i), known as the Rayleigh criterion, allows one to avoid effects of Anderson localization [10]. Condition (ii) stems from the fact that diffusion cannot adequately describe processes on scales comparable to ℓ [3]. Finally, condition (iii) precludes quasi-1D localization [6].

In defining a projection to one dimension, it is instructive to take a step back by writing Eq. (1) as a combination of the diffusive flux $\mathbf{J}(\mathbf{r}, \mathbf{r}', t)$ and the continuity equations:

$$\mathbf{J}(\mathbf{r}, \mathbf{r}', t) = -D_0 \nabla_{\mathbf{r}} G(\mathbf{r}, \mathbf{r}', t), \quad (2)$$

$$\begin{aligned} \frac{\partial G(\mathbf{r}, \mathbf{r}', t)}{\partial t} + \nabla_{\mathbf{r}} \cdot \mathbf{J}(\mathbf{r}, \mathbf{r}', t) + \frac{1}{\tau_a} G(\mathbf{r}, \mathbf{r}', t) \\ = S_0(t) \delta(\mathbf{r} - \mathbf{r}'). \end{aligned} \quad (3)$$

As the first step, we will perform an average over the position of the source \mathbf{r}' in the cross-section plane at a fixed depth z' as $A^{-1}(z') \int_{A(z')} d\boldsymbol{\rho}' \times$, where $\boldsymbol{\rho}'$ is the transverse coordinate at z' :

$$\mathbf{J}(\mathbf{r}, z', t) = -D_0 \nabla_{\mathbf{r}} G(\mathbf{r}, z', t), \quad (4)$$

$$\begin{aligned} \frac{\partial G(\mathbf{r}, z', t)}{\partial t} + \nabla_{\mathbf{r}} \cdot \mathbf{J}(\mathbf{r}, z', t) + \frac{1}{\tau_a} G(\mathbf{r}, z', t) \\ = S_0(t) \delta(z - z')/A(z'). \end{aligned} \quad (5)$$

$G(\mathbf{r}, z', t)$ represents the ensemble-averaged intensity at point \mathbf{r} with a planar source $S_0(t)/A(z')$ at z' .

The divergence operator in Eq. (5) presents a challenge while performing averaging over the cross-section coordinate $\boldsymbol{\rho}$ in $\mathbf{r} \equiv (\boldsymbol{\rho}, z)$. Instead, we accomplish this task by performing integration over *volume* sandwiched between cross sections at z and $z + \Delta z$; see Fig. 1. Using the Gauss theorem,

the volume integration is reduced to surface integration,

$$\oint_V \nabla_{\mathbf{r}} \cdot \mathbf{J}(\mathbf{r}, z', t) d\mathbf{r} = \int_S \mathbf{J}(\mathbf{r}, z', t) \cdot \mathbf{n} d\sigma. \quad (6)$$

In the next step we separate the surface integral into three parts: a ring over the surface of the waveguide, and two cross sections: at z and $z + \Delta z$. The first contribution vanishes due to the absence of the normal component of the flux at the boundary. The remaining two contributions to Eq. (6) are computed as follows:

$$\begin{aligned} - \int_{A(z)} J_z(\boldsymbol{\rho}, z, z', t) d\boldsymbol{\rho} + \int_{A(z+\Delta z)} J_z(\boldsymbol{\rho}, z + \Delta z, z', t) d\boldsymbol{\rho} \\ \simeq \frac{1}{A(z)} \frac{\partial}{\partial z} [A(z) J_z(z, z', t)] \times A(z) \Delta z, \end{aligned} \quad (7)$$

where the subscript z denotes the longitudinal component (of flux) and $J_z(z, z', t) \equiv A^{-1}(z) \int_{A(z)} J_z(\boldsymbol{\rho}, z, z', t) d\boldsymbol{\rho}$ is the cross section average. In Eq. (7) we accounted, in the leading order of Δz , for two possible sources of change in the value of the integral—one due to $\partial J_z(z, z', t)/\partial z$ and the other due to the variability of the waveguide shape $dA(z)/dz$. Last, the volume integration of remaining terms in Eq. (5) does not pose problems, reducing them to the cross-sectional averages, e.g., $\oint_V G(\mathbf{r}, z', t) d\mathbf{r} \simeq \Delta z \times \int_{A(z)} G(\boldsymbol{\rho}, z, z', t) d\boldsymbol{\rho} \equiv G(z, z', t) \times [A(z) \Delta z]$.

Examining Eq. (7), we see that completion of our task of reducing the higher-dimensional problem to one dimension requires an expression for the longitudinal flux, $J_z(z, z', t)$. Cross-sectional (surface) integration of the z component of Eq. (4) yields $J_z(z, z', t) \simeq -D_0 \partial G(z, z', t)/\partial z$ assuming $W'(z)$ is small. Upon substitution into Eqs. (7) and (5) we obtain

$$\begin{aligned} \frac{\partial G(z, z', t)}{\partial t} - \frac{1}{A(z)} \frac{\partial}{\partial z} \left[D_0 A(z) \frac{\partial G(z, z', t)}{\partial z} \right] \\ + \frac{1}{\tau_a} G(z, z', t) = \frac{S_0(t)}{A(z)} \delta(z - z'). \end{aligned} \quad (8)$$

The above expression, together with similarly obtained boundary conditions $[z_0 \partial G(z, z', t)/\partial z \mp G(z, z', t)]_{z=0,L} = 0$, represents the final result of this section.

We would like to finish this discussion by putting our result in context of the available literature. Particle diffusion in confined geometries is a common problem in physical chemistry; see for example Ref. [22] for a review. In this problem, it is convenient to define a cross-section integrated quantity, as opposed to the cross-section averaged $G(z, z', t)$ in Eq. (8), representing linear density $c(z, t)$ of, e.g., a solute. The governing equation

$$\frac{\partial c(z, t)}{\partial t} - \frac{\partial}{\partial z} \left[D_0 A(z) \frac{\partial c(z, t)}{\partial z} \frac{1}{A(z)} \right] = 0 \quad (9)$$

is known as the Fick-Jacobs equation. It has been derived by Jacobs [39] heuristically based on the particle conservation argument, Zwanzig [40] via reducing higher dimensional Smoluchowski equation to one dimension, and by others [41,42]. Without the additional source and absorption terms in the case of the wave diffusion, Eqs. (8) and (9) agree. We are not aware of reports of derivation such as the one presented

above, in particular, in the context of wave diffusion where there is no particle conservation constraint.

In the context of particle diffusion, there was a considerable effort to evaluate the validity of the projection (reduction) to one dimension via Eq. (9). It has been found [40–43] that even for rapidly varying channel profiles with $dW(z)/dz \sim 1$, a reliable solution can be obtained from a modified Fick-Jacobs equation with $D_0 \rightarrow D_0 \times [1 + W'^2(z)]^{-\alpha}$, where $\alpha = 1/3, 1/2$ in two and three dimensions respectively. Hence, we surmise that a similar substitution should extend the validity of Eq. (8) as well.

A stationary version of the diffusion equation reduces to a generic Poisson equation, which is common in different branches of physics. As such, it can describe eigenmodes of sound in an ideal fluid in a rigid tube (e.g., a horn or a gramophone), transverse vibrations of a string of varying cross section, etc. [44]. Reduction to one dimension in these problems, known as the Webster equation [45], has a long history with the original contributions due to Bernoulli, Lagrange, Euler, Heaviside, and Rayleigh; see Ref. [46] for a historical review of early works. Such a reduction works well in the “low-frequency” limit [47,48], i.e., solutions which vary sufficiently slowly in space. This is consistent with approximations in the Fick-Jacobs equation, where the very process of diffusion tends to smooth out any rapid variation of concentration/intensity. In acoustics, the reduction to one dimension has been extended to include processes of dissipation [48] and the inverse design [46] considered in a different context in this work.

Having completed the derivation of Eq. (8), in the remainder of this work we will consider its static version (i.e., without the time-derivative term) to compute the long-range spatial correlation of intensity.

III. INTENSITY CORRELATION IN DISORDERED WAVEGUIDES WITH VARYING CROSS SECTION

Intensity correlations originate from interference in wave scattering and propagation. It was first considered for electronic waves in mesoscopic physics [9,14,49,50]. The electromagnetic waves, such as visible light or microwaves, offer a convenient testbed for the study of correlation with numerous practical applications [3,11,16,17,51,52]. For the incident plane wave, the spatial correlation is defined as

$$C(\mathbf{r}_1, \mathbf{r}_2) = \frac{\langle \delta I(\mathbf{r}_1) \delta I(\mathbf{r}_2) \rangle}{\langle I(\mathbf{r}_1) \rangle \langle I(\mathbf{r}_2) \rangle}, \quad (10)$$

where $\langle \dots \rangle$ denotes the ensemble average and $\delta I(\mathbf{r}) = I(\mathbf{r}) - \langle I(\mathbf{r}) \rangle$ is the deviation of intensity from its average at \mathbf{r} . This arrangement implies adding contributions from all trajectories originating from the front surface, i.e., at all possible $R_{1,2}$ in Fig. 1.

Three universal, i.e., independent of the microscopical details of the disorder, contributions to $C(\mathbf{r}_1, \mathbf{r}_2)$ have been identified [3,9,53]: short-range C_1 describing a speckle pattern, long-range C_2 leading to, e.g., fluctuations of total transmission, and an infinite range C_3 underlying the universal conductance fluctuation [11,54,55]. Diagrammatically, interferences between waves scattered along independent paths

give rise to C_1 , one crossing of paths shown in Fig. 1 generates C_2 , and two crossings cause C_3 . The spatial correlation term $C_1(\mathbf{r}_1, \mathbf{r}_2)$ has unit magnitude at $\mathbf{r}_1 = \mathbf{r}_2$ but decays quickly when $|\mathbf{r}_1 - \mathbf{r}_2|$ exceeds the speckle size. $C_2(\mathbf{r}_1, \mathbf{r}_2) \propto 1/g$ but decays much more slowly, while $C_3(\mathbf{r}_1, \mathbf{r}_2) \propto 1/g^2$ is a constant value. The dimensionless conductance g is assumed to be large in diffusive systems considered here.

Serendipitously, averaging over the cross section of the waveguide, such as that performed by the projection technique in the previous section, allows one to obtain the long-range correlation in the leading order of $1/g$ [19,20]. Indeed, averaging over the cross section reduces the contribution of the short-range C_1 correlation by the factor $1/N$ (N is the number of waveguide modes), whereas the contribution of $C_2 \propto 1/g$ remains unaffected because it is present at any value of the transverse coordinate. The ratio of their magnitudes is $g/N \propto \ell/L \ll 1$ for a strongly scattering system, where L is the length of the waveguide. Meanwhile, the contribution of the C_3 term remains smaller, at the level of $1/g^2$. Therefore, we conclude that

$$C_2(z_1, z_2) \simeq \frac{\langle \delta I(z_1) \delta I(z_2) \rangle}{\langle I(z_1) \rangle \langle I(z_2) \rangle}. \quad (11)$$

As seen above, the projection technique is perfectly suited for calculation of the long-range correlation, which we undertake next. We begin with an expression first obtained with the Langevin approach [15,56]:

$$C_2(\mathbf{r}_1, \mathbf{r}_2) = a_d D_0^2 \frac{\int_V \langle I(\mathbf{r}) \rangle^2 \nabla_{\mathbf{r}} G(\mathbf{r}_1, \mathbf{r}) \cdot \nabla_{\mathbf{r}} G(\mathbf{r}_2, \mathbf{r}) d\mathbf{r}}{\langle I(\mathbf{r}_1) \rangle \langle I(\mathbf{r}_2) \rangle}. \quad (12)$$

Here, $G(\mathbf{r}, \mathbf{r}')$ is the Green’s function of the static version of the diffusion equation (1) with a constant source $S_0(t) \equiv 1$. $a_2 = 4/k\ell$ and $a_3 = 6\pi/k^2\ell$ are the dimensionality dependent coefficients. Equation (12) has a transparent diagrammatic interpretation. In this expression, $\langle I(\mathbf{r}) \rangle^2$ represents two diffusive paths connecting the input surface of the waveguide to a crossing point at \mathbf{r} ; Green’s functions $G(\mathbf{r}_{1,2}, \mathbf{r})$ describe the diffuse propagation from \mathbf{r} to the detectors at $\mathbf{r}_{1,2}$; and the gradient operators together with the constant prefactors originate from the interference (i.e., Hikami box) at \mathbf{r} . Finally, volume integration over \mathbf{r} signifies averaging over all possible locations of interference.

Cross-sectional average of $\langle I(\mathbf{r}_{1,2}) \rangle$ terms in the denominator of Eq. (12) does not present challenges due to their weak dependence on the transverse coordinates, i.e., $\langle I(\mathbf{r}) \rangle \simeq \langle I(z) \rangle$. To proceed with the analytical calculation of Eq. (12), we average the nominator over the transverse components of \mathbf{r}_1 and \mathbf{r}_2 . Although $\nabla_{\mathbf{r}} G(z_1, \mathbf{r}) \cdot \nabla_{\mathbf{r}} G(z_2, \mathbf{r})$ includes derivatives of the Green’s functions with respect to both longitudinal and transverse coordinates, the former makes the dominant contribution. Indeed, because the arguments of a Green’s function can be swapped, $\nabla_{\mathbf{r}} G(z_1, \mathbf{r})$ can be viewed as $\nabla_{\mathbf{r}} G(\mathbf{r}, z_{1,2})$. In this form, $G(\mathbf{r}, z)$ represents intensity at point \mathbf{r} with a uniform planar source at the cross section z . Such a source should not produce large transverse variation of intensity as long as the cross section is not changing too

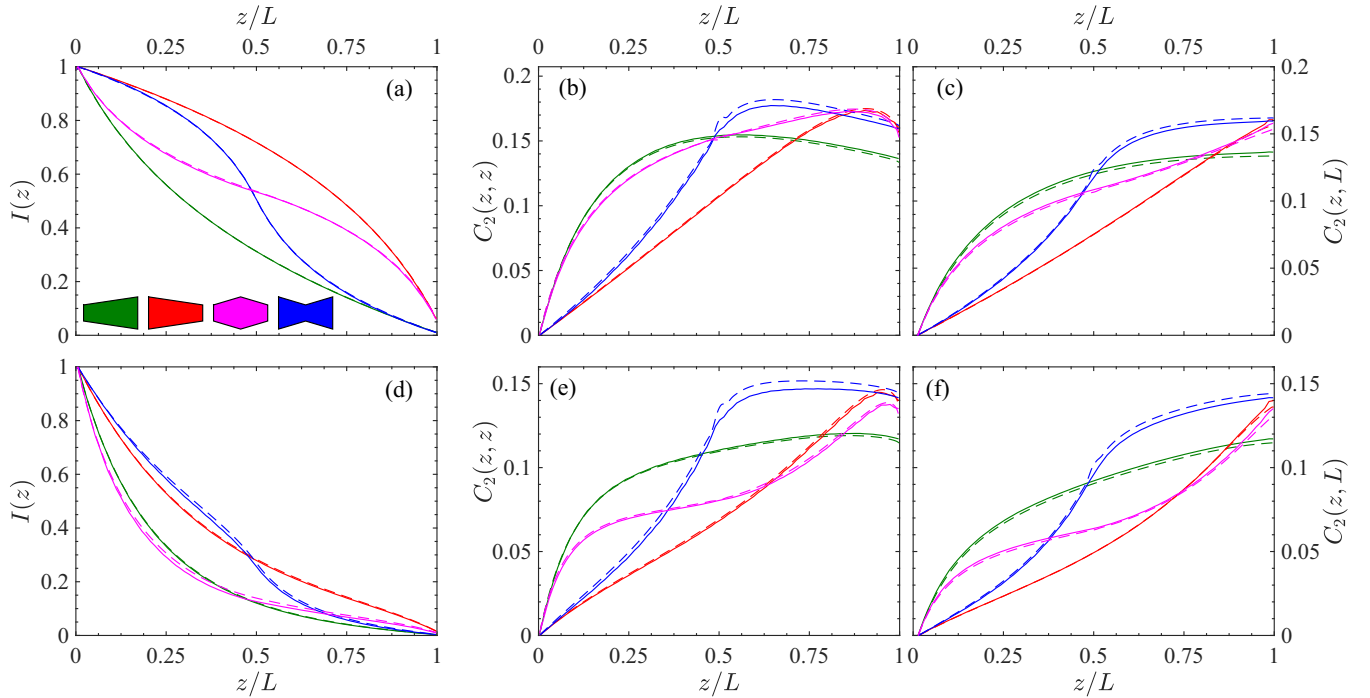


FIG. 2. Intensity and the long-range correlation computed using 2D calculations (solid lines) and projection to 1D technique (dashed lines). Line color corresponds to one of the four waveguide shapes depicted in the inset of panel (a). Passive/absorbing waveguides are shown in (a)–(c) and (d)–(f) respectively; see text for system parameters.

rapidly, i.e., $dW(z)/dz < 1$. Hence, we obtain

$$C_2(z_1, z_2) \simeq a_d D_0^2 \frac{\int_0^L \frac{\partial G(z_1, z)}{\partial z} \frac{\partial G(z_2, z)}{\partial z} \langle I(z) \rangle^2 A(z) dz}{\langle I(z_1) \rangle \langle I(z_2) \rangle}, \quad (13)$$

where $G(z, z')$ is the solution of the static version of the diffusion equation [with a constant source $S_0(t) \equiv 1$] we obtained previously using projection technique; cf. Eq. (8). $\langle I(z) \rangle$ is the solution of the same equation with $S_0(t) \equiv 0$, and a constant value at $z = 0$, as will be discussed in the next section. Equation (13) together with the static version of Eq. (8) have rather broad applicability, for example, they can incorporate the effects of absorption or gain on the correlations [20,57].

In Fig. 2, we test the applicability of the projection technique for lossless (a)–(c) and absorbing (d)–(f) cases in four different 2D waveguides, schematically shown in inset of panel (a). First, the intensity and Green's function were obtained via direct numerical solution of the 2D diffusion equation using Comsol Multiphysics solver. The long-range correlation was obtained by averaging the nominator and denominator of Eq. (12) over the cross section as in Ref. [20]. These 2D results are shown as solid lines in Fig. 2. In the second method, we employed the projection technique by using Eq. (8) (without time dependence) to compute 1D intensity and Green's function. By substituting these into Eq. (13) we obtained the projection (1D) results, shown as dashed lines in Fig. 2. We used the following system parameters: $L/\ell \simeq 35$, $W_{\min}/L = 1/8$ and $W_{\max}/L = 3/4$, and $kl \simeq 26$. For absorbing systems in Figs. 2(d)–2(f), we used diffusion absorption length $\xi_a \simeq L/3$. As it can be seen from Fig. 2, the projection technique works well for both cross-section average intensity and the long-range correlation with and without absorption.

IV. ANALYTICAL RESULT FOR LONG-RANGE CORRELATIONS IN LOSSLESS DISORDERED WAVEGUIDES

In this section we demonstrate that, without absorption, the long-range intensity correlation can be obtained in a closed form for an arbitrary slow-varying [$dW(z)/dz < 1$] waveguide geometry. To that end, we introduce a change of spatial variable,

$$\zeta(z) = \frac{\frac{z_0}{A(0)} + \int_0^z \frac{d\bar{z}}{A(\bar{z})}}{\frac{z_0}{A(0)} + \int_0^L \frac{d\bar{z}}{A(\bar{z})} + \frac{z_0}{A(L)}}. \quad (14)$$

In terms of this variable, the defining equation for Green's function takes a simple form,

$$-\frac{\partial^2 G(\zeta, \zeta')}{\partial \zeta^2} = \delta(\zeta - \zeta'), \quad (15)$$

with constant factors absorbed in the definition of the Green's function to make it dimensionless. Furthermore, extending the region of applicability of ζ from $\zeta_0 \leq \zeta \leq \zeta_L$ to $0 \leq \zeta \leq 1$ allows us to simplify boundary conditions to $G(\zeta, \zeta')|_{\zeta=0,1} = 0$. Here ζ_0 and ζ_L are defined by inserting $z = 0$ and L in Eq. (14) respectively. Equation (13) for the long-range correlation takes the form

$$C_2(\zeta_1, \zeta_2) \simeq \tilde{a}_d \frac{\int_{\zeta_0}^{\zeta_L} \frac{\partial G(\zeta_1, \zeta)}{\partial \zeta} \frac{\partial G(\zeta_2, \zeta)}{\partial \zeta} \langle I(\zeta) \rangle^2 d\zeta}{\langle I(\zeta_1) \rangle \langle I(\zeta_2) \rangle}, \quad (16)$$

where $\langle I(\zeta) \rangle$ satisfies the homogeneous version of Eq. (15) with $\langle I(\zeta_0) \rangle = I_0$ and $\langle I(1) \rangle = 0$ boundary conditions, and $\tilde{a}_d = a_d \times [z_0/A(0) + \int_0^L A^{-1}(z) dz + z_0/A(L)]$.

The final expression for the long-range correlation can now be obtained substituting the solution of Eq. (15),

$$G(\zeta, \zeta') = \begin{cases} \zeta(1 - \zeta'), & \zeta < \zeta' \\ \zeta'(1 - \zeta), & \zeta > \zeta' \end{cases} \quad (17)$$

and the corresponding intensity as $\langle I(\zeta) \rangle = I_0(1 - \zeta)/(1 - \zeta_0)$ into Eq. (16). We obtain

$$C_2(\zeta_1, \zeta_2) = \frac{2}{3g} \left[\zeta_1(2 - \zeta_1) + \frac{\zeta_1}{1 - \zeta_1}(1 - \zeta_2)^2 \right], \quad (18)$$

where $\zeta_{1,2} \equiv \zeta(z_{1,2})$ as defined by Eq. (14), and the dimensionless conductance is introduced via $g = 2/\tilde{a}_d$. When $\zeta_1 = \zeta_2$, Eq. (18) yields

$$C_2(\zeta, \zeta) = \frac{2\zeta}{g} \left(1 - \frac{2\zeta}{3} \right). \quad (19)$$

This quantity corresponds to the leading non-Rayleigh contribution to the fluctuation of intensity and originates in the nonlocality of wave transport. Both Eqs. (18) and (19) reduce to known expressions for waveguides with constant cross section, in this case $\zeta(z) = (z + z_0)/(L + 2z_0)$, which can be found from Eq. (14).

We would like to point out several general properties of Eqs. (18) and (19) that are common to all waveguides irrespective of their shape. For the sake of simplicity, we will assume that small corrections $z_0/L \sim \ell/L \ll 1$ can be neglected. We find that $g = (2/a_d)/[\int_0^L A^{-1}(z)dz]$; $C_2(L, L) = 2/(3g)$; the maximum value of the correlation $\max[C_2(\zeta_1, \zeta_2)] = C_2(\zeta_{\max}, \zeta_{\max}) = (9/8) \times 2/(3g)$, where $\zeta_{\max} = 3/4$. $C_2(\zeta, \zeta)$ is a monotonically increasing function of ζ between 0 and ζ_{\max} and a monotonically decreasing between ζ_{\max} and 1. Furthermore, $C_2(\zeta, \zeta) \leq 2/(3g)$ for $0 \leq \zeta \leq (1/2)$ and $2/(3g) \leq C_2(\zeta, \zeta) \leq 3/(4g)$ in the interval for $(1/2) \leq \zeta \leq 1$. Remarkably, $C_2(\zeta, \zeta)$ varies by less than 12% in the second interval. The long-range correlation between the output intensity at $\zeta_2 = 1$ and that in the interior of the sample is $C_2(\zeta, 1) = 2/(3g)\zeta(2 - \zeta)$. It decays monotonically with distance from the output surface, however, the rate of the decay is determined by the $\zeta(z)$, which is set by the shape of the waveguide. In a waveguide with constant cross section, $C_2(z, L) \simeq 2/(3g)z/L[2 - z/L]$ in agreement with Ref. [56].

Equation (18) also predicts correlation between intensities at $z = 0, L$ surfaces. In this case, z_0 terms cannot be neglected as they make the leading contribution to ζ_0 and, therefore, have to be retained. Evaluation of $C_2(\zeta_0, \zeta_L)$ gives $2/(3N_0)$ in both two and three dimensions, where N_0 is the number of waveguide modes at the input cross section $z = 0$. Correlation between the transmitted and reflected intensities has been studied theoretically [58,59] and experimentally [60]. It was found to be negatively correlated at the level of $-2/(3N_0)$. Because an increase of intensity at the front surface (positive correlation) corresponds to a reduction (negative correlation) of the reflected intensity, our results are in agreement with Ref. [59]. In addition, the maximum value of $C_2(z_{\max}, z_{\max}) = (9/8) \times 2/(3g)$ is independent of the extrapolation length z_0 . The leading term for $C_2(0, 0) \simeq 1/N_0$ corresponds to addition of N_0 uncorrelated modes. In contrast, at output surface, the leading correction is $C_2(L, L) \simeq 2/(3g) + 1/(3N_L)$, where N_L is the number of modes at the output.

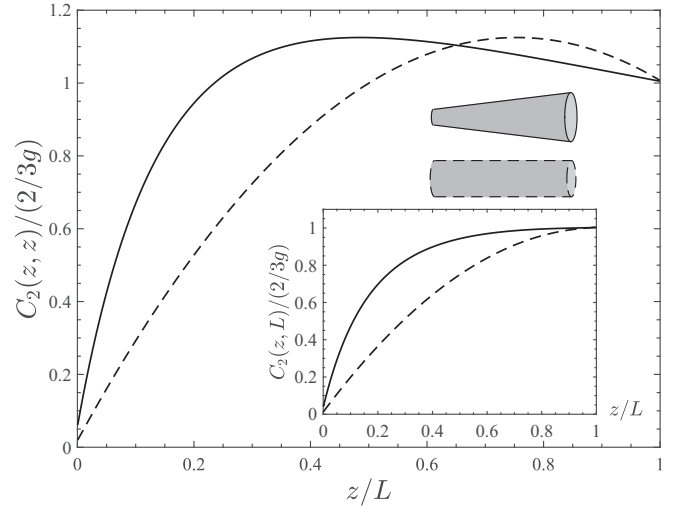


FIG. 3. Solid line in the main panel depicts $C_2(z, z)$ in a 3D expanding disordered waveguide shown in the inset; see text for system parameters. The dashed line depicts the same quantity for a 3D cylindrical waveguide of constant width. The inset plots the long-range correlation $C_2(z, L)$ for the two cases in the main plot.

Figure 3 illustrates the dependence of the correlation on the shape of the waveguide by plotting $C_2(z, z)$ and $C_2(z, L)$ for an expanding disordered waveguide, in which the diameter $W(z)$ is a linear function of z . We used the following parameters: $L = 100\ell$, $k\ell = 10$, $A(0) = 100\ell^2$, $A(L) = 1000\ell^2$, $z_0 = (2/3)\ell$, that correspond to $g \simeq 33$. For comparison, we also plot with a dashed line the same quantities for the waveguide of constant width equal to $A = 550\ell^2$, in this case $g = 58$. We can clearly see that the shape of the waveguide can have a significant effect on the correlation. Specifically, the reduced width at the front end led to a steeper increase of both $C_2(z, z)$ and $C_2(z, L)$ for small z . This dependence can be deduced, e.g., from Eq. (19) as $dC_2(z, z)/dz \propto \zeta'(z) \propto A^{-1}(z)$ for $\zeta \ll 1$. Therefore, narrower opening of the linearly expanding waveguide leads to a steeper increase of correlation in the first half of the sample in Fig. 3. Since the maximum correlation is bounded from above by the value $3/4g$, a rapid increase at the beginning of the waveguide inadvertently leads to a weaker dependence towards $z = L$. In the case of $C_2(z, z)$, as was discussed above, once the maximum value of $3/4g$ is reached at z_{\max} , in the remainder of the system the function varies in only a narrow range, $2/3g \leq C_2(z, z) \leq 3/4g$; see Fig. 3.

To conclude this section, we note that since $\zeta(z)$ is determined by $A(z)$ via Eq. (14), one can exploit the freedom of choice in the shape of the waveguide in order to predictably manipulate the correlation, within the constraints imposed by the general properties above. We tackle this task below.

V. INVERSE DESIGN OF THE LONG-RANGE CORRELATION

The compact-form analytical expression given in Eq. (18) establishes a relation between shape of the diffusive waveguide and correlation $C_2(z_1, z_2)$ of the cross-section averaged intensity, thus enabling the predictive (inverse) design. Two comments are in order. First, $C_2(z_1, z_2)$ is the function of

two variables (z_1 and z_2) whereas $A(z)$ is of one, so the mapping cannot generally be defined. To circumvent this problem, we are going to consider two possible mappings: one from the diagonal (fluctuation) $C_2(z, z)$, and the other from the off-diagonal (correlation) $C_2(z, L)$ functions. The second comment concerns the constraints imposed on possible $C_2(z, z)$ and $C_2(z, L)$. Indeed, as discussed in previous sections, see also Fig. 3, neither of the two mappings allow an arbitrary function form. For example, neglecting z_0 , $C_2(z, z)$ has to be monotonically increasing from 0 to a maximum and then monotonically decreasing to 8/9 of the maximum value at the output. Likewise, $C_2(z, L)$ has to be a monotonically increasing function of z . Below, we obtain such constrained mappings.

Solving Eq. (19) for ζ and then inverting $\zeta(z)$ with the help of Eq. (14) we obtain

$$A(z) = a_d \frac{\sqrt{1 - \frac{4g}{3}C_2(z, z)}}{\left| \frac{dC_2(z, z)}{dz} \right|}. \quad (20)$$

The structure of this relationship is intimately related to the constraints we imposed on $C_2(z, z)$. Indeed, the $4g/3$ factor ensures that the expression under the square root remains positive or zero. The latter case corresponds to the maximum of the function at z_{\max} , where both the nominator and denominator of Eq. (20) turn to zero simultaneously. To prevent $A(z)$ from turning to zero or having a singularity, we need to ensure that $C_2(z, z)$ has a parabolic behavior in the vicinity of its maximum.

Following steps similar to those used to arrive at Eq. (20), we find

$$A(z) = \frac{2a_d}{3} \frac{\sqrt{1 - \frac{C_2(z, L)}{C_2(L, L)}}}{\left| \frac{dC_2(z, L)}{dz} \right|}. \quad (21)$$

Unlike Eq. (20), where the maximum value of the input function was related to conductance using a simple relationship, the maximum value of $C_2(z, L)$ at $z = L$ is only approximately equal to $2/(3g)$ with additional (smaller) corrections due to the finite extrapolation length z_0 . Hence, normalization by $C_2(L, L)$ guarantees that the expression under the square root does not fall below zero. Similar to Eq. (20), the vanishing of $dC_2(z, L)/dz$ in Eq. (21) at $z = L$ coincides with a zero of the nominator, preventing a singularity.

Equations (20) and (21) open a possibility of inverse design. As an example, we design a waveguide where the diagonal term $C_2(z, z)$ is a (nearly) piecewise linear function. As discussed in previous sections, a choice of model correlations has several constraints. Therefore, we set out to find a functional form of $A(z)$, such that

$$C_2(z, z) = \begin{cases} \frac{z}{z_c} \times \frac{3}{4g}, & z < z_c \\ \frac{L-z}{L-z_c} \times \frac{1}{12g} + \frac{2}{3g}, & z > z_c \end{cases}, \quad (22)$$

where we neglected the small corrections at $z = 0, L$ due to the extrapolation effect. This function was chosen to satisfy the following constraints: (i) it monotonically increases in $0 < z < z_c$; (ii) it monotonically decreases in $z_c < z < L$; (iii) it maximum value is $3/4g$ at z_c ; and (iv) its value is $2/3g$ at $z = L$. However, the model function does not have

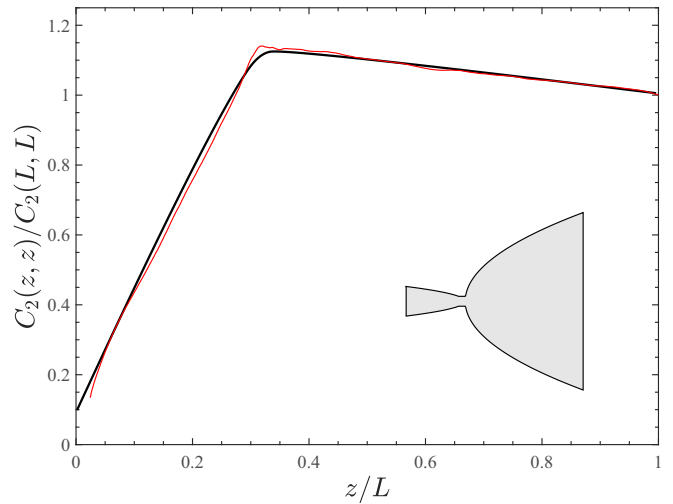


FIG. 4. Thick solid line in the main plot depicts $C_2(z, z)$ in a two-dimensional expanding disordered waveguide defined by Eq. (23). Thin line is the result of numerical simulation. The inset plots the shape of the considered waveguide.

a vanishing derivative at its maximum at z_c . This should result in an artifact to be corrected at a later step. Substitution of Eq. (22) into Eq. (20) gives

$$A(z) = \frac{4ga_d}{3} \begin{cases} \sqrt{(z_c - z)z_c}, & z < z_c \\ 3\sqrt{(z - z_c)(L - z_c)}, & z > z_c \end{cases}. \quad (23)$$

We observe that Eq. (23) predicts a zero cross section at z_c . To avoid this artifact, related to a cusp in the input function in Eq. (22), we add a condition that $A(z)$ does not fall below a certain minimum value of A_{\min} .

To test the above prediction we substitute Eq. (23) into Eqs. (14) and (18) to compute the long-range correlation in a two-dimensional disordered waveguide with parameters quoted below. The thick solid line in Fig. 4 shows that the $C_2(z, z)$ is indeed close to a piecewise linear function. The deviations from the design in Eq. (22) can be seen at $z \sim 0$ and $\sim z_c$. The former is due to the fact that the model equation did not explicitly account for the extrapolation length z_0 . Replacement of a cusp-behavior at z_c with a smooth parabolic maximum is related to the structure of Eq. (20) as well as our requirement that $A(z)$ to be always greater than A_{\min} . One can see from Fig. 4, however, that this did not cause significant deviation from linearity away from the maximum.

To further verify the predictions of our inverse-design procedure, we performed numerical simulations. We consider a two-dimensional waveguide where $A(z) = W(z)$, and use the following parameters: $N_0 = 125$, $L/\ell \simeq 30$, $W(0)/\ell \simeq 5$, $W_{\min}/W(0) = 1/3$, $z_c = L/3$, and $g \simeq 7$. The simulations were performed using the method described in detail in our previous works [23,32,61]. The cross-section averaged intensity was obtained numerically by solving the wave equation and then was used to compute $C(z_1, z_2)$ using Eq. (11). The angular brackets represent the average over 1000 disorder realizations. The transport mean free path was obtained by computing the dimensionless conductance for a rectangular waveguide and then using relationship

$g = (\pi/2)N\ell/(L + 2z_0)$, where N is the number of waveguide modes. This allowed us to express all length scales in terms of ℓ , with the numerical values quoted above.

Equation (11) holds only approximately, because averaging over the cross section of the waveguide does not fully remove other contributions. In order to compare the numerical simulation with our theoretical prediction, which only accounts for the C_2 contribution, we removed the following two residuals. The first is related to the C_1 contribution and can be evaluated by noticing that cross-sectional averaging of intensities in $W^{-2}(z) \iint \langle \delta I(z_1, y) \delta I(z_2, y + \Delta y) \rangle dy d\Delta y$ has a small but z -dependent contribution, which can be computed as

$$C_1(z, z) \simeq \frac{1}{W(z)} \int_0^{W(z)} C_1(\Delta y) d\Delta y. \quad (24)$$

Away from boundaries $z \sim 0, L$, the short-range correlation [18,49] $C_1(\Delta y)$ can be evaluated in two dimensions in terms of the Bessel function [62] as $J_0^2(k\Delta y)$. The second residual is related to another type of correlation, C_0 [63], which is nonuniversal. This contribution has been related to the variance of the local density of states [64,65], which we compute directly in our numerical simulations. The magnitudes of the two contributions are determined by $1/(kW)$ and $1/(k\ell)$, respectively. Therefore, in larger systems and, particularly in three-dimensional systems, these residuals are expected to be negligible.

The thin line in Fig. 4 shows the results of the numerically computed $C_2(z, z)$ after subtracting the two residual contributions described above. As predicted by Eq. (22), $C_2(z, z)$ exhibits nearly linear dependence in both $0 < z < z_c$ and $z_c < z < L$ intervals. We attribute the deviation in the $z \sim 0$ region to the remaining ballistic intensity of the incident waves.

VI. CONCLUSIONS

In this work, we first present a method to compute the Green's function of the diffusion equation in two- and three-dimensional disordered waveguides with slow-varying shape.

This is accomplished by reducing the dimensionality of the problem to one dimension. Because geometry dependence of the long-range intensity correlations arises from such dependence in Green's functions, the complexity of the problem of determining the correlations is greatly reduced. Furthermore, in the case of lossless media, we are able to obtain close-form analytical expression for both the Green's function and the long-range correlation in arbitrary geometry. This relationship allows us to design specific waveguide shapes with unusual pre-determined nonlocal correlations, which we confirm with the direct numerical simulations. We refer to this approach as an inverse design. It is worth noting that the possibility of inversion of the *nonlocal long-range* correlations via the rather simple Eqs. (20) and (21) is not trivial.

Experimental measurement of the long-range correlation in our previous work [20] in photonic disordered waveguides already showed shape dependence. The results agreed with theoretical predictions based on Eq. (12). In waveguides other than rectangular, we had to resort to numerical calculation of the full two-dimensional Green's function. Although samples in Ref. [20] exhibited absorption and our analytical results for passive systems in the last section do not apply, Eq. (13) does. Therefore, results of this work offer a much simpler approach based on the projection technique.

Our technique of studying geometry dependence of intensity correlations can be extended to studying other interference phenomena such as localization-induced position-dependent diffusion, transmission eigenchannels, etc.; see, e.g., Refs. [8,23,66]. Our results are applicable to electronic, acoustic, electromagnetic, and other types of waves and can incorporate the effect of absorption or optical gain.

ACKNOWLEDGMENTS

The authors acknowledge support from the U.S. National Science Foundation under Grants No. DMR-1205223 and No. DMR-1205307. We would like to thank an anonymous referee for drawing our attention to a connection to works on horns in acoustics.

-
- [1] P. M. Morse and H. Feshbach, *Methods of Theoretical Physics* (McGraw-Hill, New York, 1953).
 - [2] A. Ishimaru, *Wave Propagation and Scattering in Random Media* (Academic, New York, 1978).
 - [3] M. C. van Rossum and T. M. Nieuwenhuizen, *Rev. Mod. Phys.* **71**, 313 (1999).
 - [4] L. V. Wang and H. Wu, *Biomedical Optics: Principles and Imaging* (Wiley-Interscience, New York, 2007).
 - [5] *Mesoscopic Phenomena in Solids*, edited by B. L. Altshuler, P. A. Lee, and R. A. Webb (North-Holland, Amsterdam, 1991).
 - [6] C. W. Beenakker, *Rev. Mod. Phys.* **69**, 731 (1997).
 - [7] A. Lagendijk, B. van Tiggelen, and D. S. Wiersma, *Phys. Today* **62**(8), 24 (2009).
 - [8] S. Rotter and S. Gigan, *Rev. Mod. Phys.* **89**, 015005 (2017).
 - [9] R. Berkovits and S. Feng, *Phys. Rep.* **238**, 135 (1994).
 - [10] P. Sheng, *Introduction to Wave Scattering, Localization and Mesoscopic Phenomena* (Springer, New York, 2006).
 - [11] E. Akkermans and G. Montambaux, *Mesoscopic Physics of Electrons and Photons* (Cambridge University Press, Cambridge, UK, 2007).
 - [12] L. P. Gor'kov, A. I. Larkin, and D. E. Khmel'nitskii, *Pis'ma Zh. Eksp. Teor. Fiz.* **30**, 248 (1979) [*JETP Lett.* **30**, 228 (1979)].
 - [13] S. Hikami, *Phys. Rev. B* **24**, 2671 (1981).
 - [14] M. J. Stephen and G. Cwilich, *Phys. Rev. Lett.* **59**, 285 (1987).
 - [15] R. Pnini and B. Shapiro, *Phys. Rev. B* **39**, 6986 (1989).
 - [16] A. Z. Genack, N. Garcia, and W. Polkosnik, *Phys. Rev. Lett.* **65**, 2129 (1990).
 - [17] A. A. Lisyansky and D. Livdan, *Phys. Rev. B* **47**, 14157 (1993).
 - [18] P. Sebbah, R. Pnini, and A. Z. Genack, *Phys. Rev. E* **62**, 7348 (2000).
 - [19] R. Sarma, A. Yamilov, P. Neupane, B. Shapiro, and H. Cao, *Phys. Rev. B* **90**, 014203 (2014).

- [20] R. Sarma, A. Yamilov, P. Neupane, and H. Cao, *Phys. Rev. B* **92**, 180203(R) (2015).
- [21] C. W. Hsu, S. F. Liew, A. Goetschy, H. Cao, and A. D. Stone, *Nat. Phys.* **13**, 497 (2017).
- [22] P. S. Burada, P. Hanggi, F. Marchesoni, G. Schmid, and P. Talkner, *Chem. Phys. Chem.* **10**, 45 (2009).
- [23] M. Koirala, R. Sarma, H. Cao, and A. Yamilov, *Phys. Rev. B* **96**, 054209 (2017).
- [24] P. A. Mosk, A. Lagendijk, G. Lerosey, and M. Fink, *Nat. Photon.* **6**, 283 (2012).
- [25] H. Yu, J. Park, K. Lee, J. Yoon, K. Kim, S. Lee, and Y. K. Park, *Curr. Appl. Phys.* **15**, 632 (2015).
- [26] X. Cheng and A. Z. Genack, *Opt. Lett.* **39**, 6324 (2014).
- [27] W. Choi, A. P. Mosk, Q. H. Park, and W. Choi, *Phys. Rev. B* **83**, 134207 (2011).
- [28] B. Gérardin, J. Laurent, A. Derode, C. Prada, and A. Aubry, *Phys. Rev. Lett.* **113**, 173901 (2014).
- [29] M. Davy, Z. Shi, J. Wang, X. Cheng, and A. Z. Genack, *Phys. Rev. Lett.* **114**, 033901 (2015).
- [30] M. Davy, Z. Shi, J. Park, C. Tian, and A. Z. Genack, *Nat. Commun.* **6**, 6893 (2015).
- [31] L. Zhao, C. Tian, Y. P. Bliokh, and V. Freilikher, *Phys. Rev. B* **92**, 094203 (2015).
- [32] R. Sarma, A. G. Yamilov, S. Petrenko, Y. Bromberg, and H. Cao, *Phys. Rev. Lett.* **117**, 086803 (2016).
- [33] O. S. Ojambati, H. Yilmaz, A. Lagendijk, A. P. Mosk, and W. L. Vos, *New J. Phys.* **18**, 043032 (2016).
- [34] O. S. Ojambati, A. P. Mosk, I. M. Vellekoop, A. Lagendijk, and W. L. Vos, *Opt. Express* **24**, 18525 (2016).
- [35] R. Sarma, A. Yamilov, and H. Cao, *Appl. Phys. Lett.* **110**, 021103 (2017).
- [36] C. W. Hsu, A. Goetschy, Y. Bromberg, A. D. Stone, and H. Cao, *Phys. Rev. Lett.* **115**, 223901 (2015).
- [37] R. Sarma, T. Golubev, A. Yamilov, and H. Cao, *Appl. Phys. Lett.* **105**, 041104 (2014).
- [38] R. Sarma, A. Yamilov, S. F. Liew, M. Guy, and H. Cao, *Phys. Rev. B* **92**, 214206 (2015).
- [39] M. H. Jacobs, *Diffusion Processes* (Springer, New York, 1967).
- [40] R. Zwanzig, *J. Phys. Chem.* **96**, 3926 (1992).
- [41] D. Reguera and J. M. Rubí, *Phys. Rev. E* **64**, 061106 (2001).
- [42] P. Kalinay and J. K. Percus, *Phys. Rev. E* **74**, 041203 (2006).
- [43] P. S. Burada, G. Schmid, D. Reguera, J. M. Rubí, and P. Hänggi, *Phys. Rev. E* **75**, 051111 (2007).
- [44] L. M. B. C. Campos, *Rev. Mod. Phys.* **58**, 117 (1986).
- [45] A. G. Webster, *Proc. Natl. Acad. Sci. USA* **5**, 275 (1919).
- [46] E. Eisner, *J. Acoust. Soc. Am.* **41**, 1126 (1967).
- [47] P. A. Martin, *J. Acoust. Soc. Am.* **116**, 1381 (2004).
- [48] L. M. Campos, *Appl. Mech. Rev.* **60**, 291 (2007).
- [49] B. Shapiro, *Phys. Rev. Lett.* **57**, 2168 (1986).
- [50] S. Feng, C. Kane, P. A. Lee, and A. D. Stone, *Phys. Rev. Lett.* **61**, 834 (1988).
- [51] J. F. de Boer, M. P. van Albada, and A. Lagendijk, *Phys. Rev. B* **45**, 658 (1992).
- [52] F. Scheffold, W. Hartl, G. Maret, and E. Matijevic, *Phys. Rev. B* **56**, 10942 (1997).
- [53] P. Sebbah, B. Hu, A. Z. Genack, R. Pnini, and B. Shapiro, *Phys. Rev. Lett.* **88**, 123901 (2002).
- [54] P. A. Lee and A. D. Stone, *Phys. Rev. Lett.* **55**, 1622 (1985).
- [55] F. Scheffold and G. Maret, *Phys. Rev. Lett.* **81**, 5800 (1998).
- [56] R. Pnini and B. Shapiro, *Phys. Lett. A* **157**, 265 (1991).
- [57] A. Yamilov, S. H. Chang, A. Burin, A. Taflove, and H. Cao, *Phys. Rev. B* **71**, 092201 (2005).
- [58] N. Fayard, A. Cazé, R. Pierrat, and R. Carminati, *Phys. Rev. A* **92**, 033827 (2015).
- [59] N. Fayard, A. Goetschy, R. Pierrat, and R. Carminati, *Phys. Rev. Lett.* **120**, 073901 (2018).
- [60] I. Starshynov, A. M. Paniagua-Diaz, N. Fayard, A. Goetschy, R. Pierrat, R. Carminati, and J. Bertolotti, *Phys. Rev. X* **8**, 021041 (2018).
- [61] A. Yamilov, S. Petrenko, R. Sarma, and H. Cao, *Phys. Rev. B* **93**, 100201(R) (2016).
- [62] A. Yamilov, *Phys. Rev. B* **78**, 045104 (2008).
- [63] B. Shapiro, *Phys. Rev. Lett.* **83**, 4733 (1999).
- [64] B. A. van Tiggelen and S. E. Skipetrov, *Phys. Rev. E* **73**, 045601(R) (2006).
- [65] M. D. Birowosuto, S. E. Skipetrov, W. L. Vos, and A. P. Mosk, *Phys. Rev. Lett.* **105**, 013904 (2010).
- [66] A. G. Yamilov, R. Sarma, B. Redding, B. Payne, H. Noh, and H. Cao, *Phys. Rev. Lett.* **112**, 023904 (2014).